
Ancient TL

www.ancienttl.org · ISSN: 2693-0935

Cunningham, A., 2016. *External beta dose rates to mineral grains in shell-rich sediment*. Ancient TL 34(1): 1-5. <https://doi.org/10.26034/la.atl.2016.498>

This article is published under a *Creative Commons Attribution 4.0 International* (CC BY):
<https://creativecommons.org/licenses/by/4.0>



© The Author(s), 2016

External beta dose rates to mineral grains in shell-rich sediment

Alastair C. Cunningham^{1*}

¹Centre for Archaeological Science, School of Earth and Environmental Sciences,
University of Wollongong, Wollongong, NSW, Australia

*Corresponding Author: acunning@uow.edu.au

Received: December 17, 2015; in final form: April 11, 2016

Abstract

Luminescence dating methods make use of the infinite-matrix assumption to simplify dose rate calculations. This works well when the sediment grain size is much smaller than the range of beta electrons in sediment (~ 3 mm). However, shell material introduces complexity in the beta dose rate calculations, because it creates low-dose-rate zones where no mineral grains are present. This phenomenon introduces an error in the estimated beta dose rate, whether or not the shells are included in the beta dose-rate measurements. The magnitude of the error depends on the size and shape of the shell material, and the quantity of it. Here, this relationship is modelled using Monte Carlo radiation transport software. The model indicates that for shell masses below 25 %, accurate estimates of beta dose rate are readily obtained from: 1) the infinite matrix dose rate of the bulk material (including shells) when shell fragments are small ($< \sim 0.001$ cm³); and 2) the infinite matrix dose rate of the sandy fraction (without shells) when shell fragments are larger ($> \sim 1$ cm³). Between these extremes of shell size, e.g. for shell-hash samples, a significant correction to the measured beta dose rate is necessary.

Keywords: luminescence, shell, carbonate, dose rate

1. Introduction

Shell material can make up a significant proportion of some types of coastal sediment. While fine shell fragments

(~ 0.001 cm³) are often present in coastal dunes, larger shell fragments (~ 0.03 cm³) can be concentrated in shell hash, forming a major part of coastal barrier sequences. Beds of whole valves and articulated shells can be laid by storm surges or tsunamis, and large concentrations of shells can be found in middens.

Optically Stimulated Luminescence (OSL) methods generally work very well for coastal sediment, but dating the shell-rich deposits presents an additional complication for the beta dose-rate calculations. The complexity arises because shell material makes the sediment non-uniform at the range of beta electrons, so invalidating the infinite-matrix assumption. As a consequence, the dose received by the dosimeter grains is less than the infinite-matrix dose (Nathan et al., 2003). While it is often possible to avoid shell-rich beds by sampling the bracketing horizons (e.g. Bateman et al., 2008), it may be necessary or desirable to target the shell-rich beds directly (e.g. Cunningham et al., 2011; Pluckhahn et al., 2015). For such sediments, OSL does have advantages over other dating methods, provided the dose-rate complications are surmounted. Radiocarbon dating and amino-acid racemization can be applied to shell material, but can be erroneous if the shell ages are not contemporary with the deposition event. For example, Oliver et al. (2015) dated a Holocene barrier sequence with quartz OSL (targeting aeolian sand beds), and found a significant offset from a previous chronology which used radiocarbon on shell hash. Radiocarbon ages of marine shells also require a reservoir correction, and terrestrial shells are problematic due to hard-water effects.

For shell-rich sediment, the disparity between the actual and infinite-matrix dose rates depends on the size and quantity of shell material. The effect can be modelled using a Monte Carlo radiation transport code, once estimates have been made of the shell size and quantity, and the radionuclide concentrations. This was done by Cunningham et al.

(2011) for a shell-rich storm-surge bed and a shell hash sample, with the OSL ages, once corrected, neatly matching the bracketing OSL dates on aeolian sand. However, such an undertaking may not be justified unless it is known that a large dose-rate correction needs to be made. If the shell content is low enough, or the shells are small enough, then the error resulting from the infinite-matrix assumption will be tolerable.

The purpose of this paper is to assess how the beta dose rate to quartz grains is influenced by the size and quantity of shell material. It is intended to help readers decide what strategy to use for beta dose-rate measurements when shells are present, and whether further modelling would be beneficial for their samples. The phenomenon of interest also affects the external beta dose to feldspar grains. However, unlike quartz grains, feldspar grains also have a significant internal beta dose, so the consequence of an error in the external beta dose rate is less severe. It is assumed here that the shell material is discrete and its composition constant over time. Complications arising from carbonate cementation and uranium uptake are discussed elsewhere (Zander et al., 2007; Nathan & Mauz, 2008).

2. The phenomenon

Typically, beta dose rate estimates follow either spectrometry or beta-counting measurements. In both cases, the sample is homogenised before measurement and the infinite-matrix (IM) assumption is used, i.e. the rate of radiation absorption is presumed equal to the rate of radiation emission (Aitken, 1985). The distribution of radionuclides is also presumed to be uniform. For sandy or silty sediments this assumption is reasonable because the range of beta particles (~ 3 mm) is much larger than the diameter of the grains (although see Guérin et al., 2012).

The introduction of shell material to the sediment creates non-uniformity in the beta field. The sediment now contains two different zones: the solid shell, and the sand matrix. Shell consists of calcite or aragonite with a density of ~ 2.70 g cm $^{-3}$. Although the density of the shell is comparable to minerals in the sand matrix, the shell does not contain any pore space. The shell material is therefore more efficient at absorbing radiation per unit volume compared to the sand matrix (mean density ~ 1.80 g cm $^{-3}$). In addition, shell material has an extremely low radionuclide concentration, providing an infinite-matrix beta dose rate of ~ 0.02 Gy ka $^{-1}$. Beta dose rates provided by the sand matrix depend on the mineralogical composition, but would typically be at least an order of magnitude larger: beta dose rates of 0.50 - 1.00 Gy ka $^{-1}$ are typical for coastal settings (e.g. van Hetteren et al., 2000; Ballarini et al., 2003).

The presence of the shell material creates zones in the sediment with low beta dose rates. The dosimeter grains, be they quartz or feldspar, are excluded from this zone, so are not subject to the lowest beta dose rates possible in the bulk sediment. The exclusion of the dosimeter grains from low-dose regions means the actual dose rate to the sand matrix is higher than the infinite-matrix dose rate. However, the

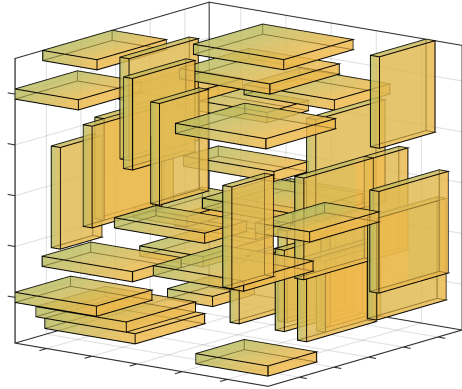


Figure 1. Example of the dimensionless model geometry. Rectangular cuboids representing the shells are added in one of the two orientations until the desired mass fraction is reached (20% in this case). Shells may not overlap, but may lie adjacent to one another.

dose rate in the sand matrix is also affected by proximity to the shells: grains closer than ~ 3 mm to a shell have a dose rate lower than the remainder of the sand matrix, because the shell is not emitting as much beta radiation as it absorbs.

This phenomenon presents a conundrum for dose rate estimation. If a shell-rich sample is homogenised before spectrometry or beta-counting measurements, then the beta dose rate to the dosimeter grains will be underestimated. However, if the shells are removed before homogenisation, then the dose rate will be overestimated because of the proximity effect. The actual beta dose rate to the grains must lie between these extremes (the bulk-sample IM dose rate, and the sand-matrix-only IM dose rate; hereafter ‘bulk-IM’ and ‘sand-IM’), and will depend on the size and quantity of the shells.

3. Monte Carlo Modelling

Monte Carlo radiation transport software simulates particle interaction in a specified geometry, with the option of recording the energy deposited in particular regions. This study uses the MCNP4C software (Briesmeister, 2000) and a simple, cellular geometry. A brief description of the model set-up is given here; full details, including sensitivity tests, are provided in the supplementary files of Cunningham et al. (2011).

The model geometry is constructed by randomly placing rectangular cuboids within a larger cube (Fig. 1). The cuboids have relative dimensions 10 : 10 : 1. The cuboids represent shells or shell fragments; they are placed in one of two orientations, until the desired volume fraction is filled with ‘shells’. The shells are given a material of CaCO $_3$, density 2.70 g cm $^{-3}$. The remaining space is defined with a material combination of SiO $_2$ and H $_2$ O and represents the sand matrix with density 1.82 g cm $^{-3}$, reflecting a water content of 5% and packing density of 65%.

Each shell, and the sand matrix, is defined as a source region for beta particles. The beta energy spectra for the sand and shell source regions are different. The spectra were generated by Cunningham et al. (2011) using gamma-spectrometry derived radionuclide concentrations for both sand and shell, which were used to weight the beta energy spectra for K, and the U and Th chains. There is a 28 : 1 ratio of energy emitted per unit mass between sand and shell. These spectra were designed for a particular coastal sample from North Holland; their use here in a generalised model is reasonable in my view, as differences in the radioactivity from sample to sample will not affect the order-of-magnitude difference between the two components.

The model has a single dosimeter, the sand-matrix region, in which the deposited energy is recorded. Particles hitting the boundary of the geometry are reflected back in random directions to maintain charged-particle equilibrium. Five different geometries were constructed with shell mass fractions of 5 %, 10 %, 20 %, 30 % and 40 %. Different shell sizes were simulated by changing the dimensions of the geometry, effectively changing the volumes of the individual shells. Each of the five geometries was used for 10 different shell volumes between 0.0001 cm³ and 2.70 cm³, resulting in 50 variations of the simulation.

4. Results

The simulation output consists of energy deposited in the sand matrix (where the dosimeter grains must be located), through the interaction of beta electrons and their secondary particles. In Fig. 2, these values are expressed as a proportion of the bulk-IM and sand-IM beta doses. Fig. 2a shows the ratio of the modelled dose to the bulk-IM dose, as a function of individual shell volume and total shell mass. The biggest departure from the bulk-IM dose occurs where shells are large and numerous. As the shell size and quantity becomes smaller, the modelled beta dose approaches the bulk-IM dose.

Fig. 2b shows the same model output, expressed as a proportion of the sand-only IM dose. When there are a small number of larger shells, the modelled dose to the sand matrix is similar to its IM dose; when there are a large number of small shell fragments, the modelled dose is much smaller than sand-IM dose.

5. Discussion

The model used here makes use of some simplifications in geometry, making the analysis easier but more limited in scope. The first limitation comes through the use of voxelisation: the shells must be placed on a discrete coordinate system. When packed densely, the shells are liable to stack on top of each other, with no intervening space for the sand matrix. This is a poor simulation of the natural sediment, where even closely packed shells are likely to have some sand grains in between. Assessed visually, the model geom-

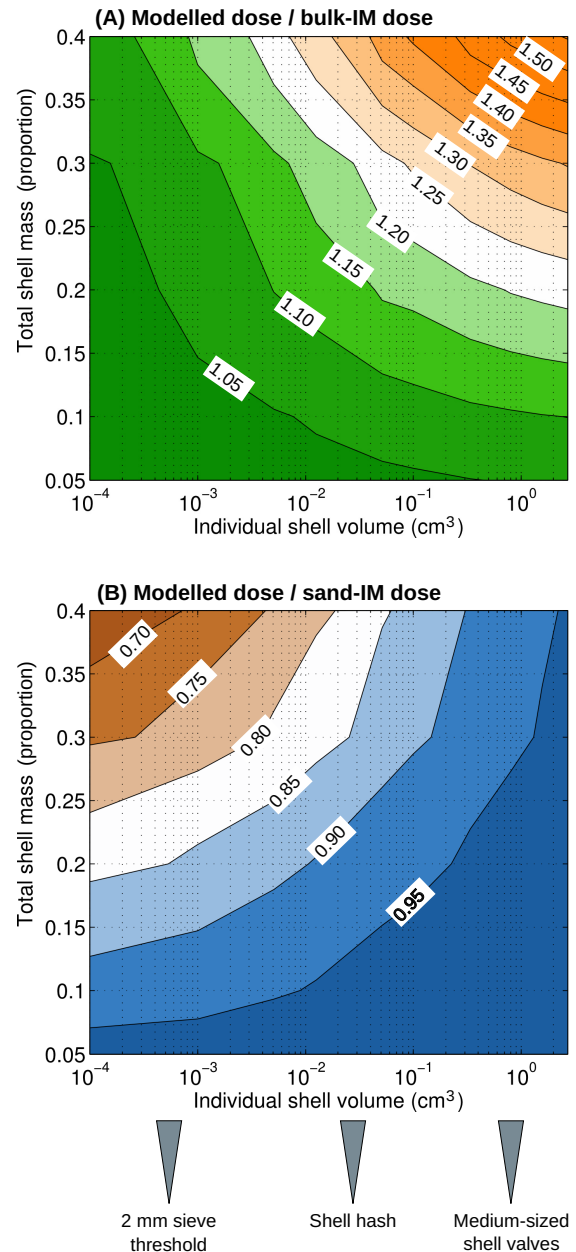


Figure 2. Results of Monte Carlo transport simulations. (a) Contour map showing the ratio of the dose received by the sand matrix to the bulk-sample infinite matrix (IM) dose, as a function of the individual shell volume and the total shell mass. (b) Contour map showing the ratio of the dose received by the sand matrix to the sand-IM dose, as a function of the individual shell volume and the total shell mass. Also indicated are the approximate volumes of medium-sized shell valves, shell hash, and the fragments around the 2 mm sieve threshold.

etry is susceptible to this effect at shell mass fractions greater than 30 % (and is responsible for the kink in the contour plots for the 30 % shell-mass simulations). The second limitation lies in the choice of shell dimensions. The dimension ratio 10 : 10 : 1 was used to approximate a medium-sized shell with length and width of 2 cm, and thickness 0.2 cm, and this ratio was kept constant for smaller shell volumes. This is not very realistic for fine shell fragments, which in nature

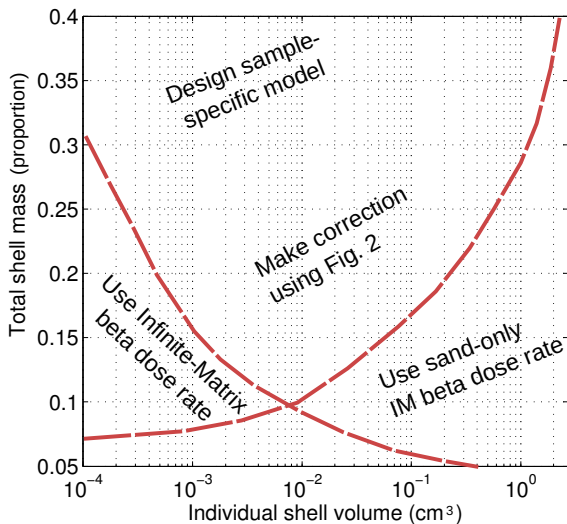


Figure 3. Visual decision guide to help choose a measurement strategy for the beta dose, as a function of the shell mass fraction and the size of the shells. Lines indicate the suggested threshold of 5% error in beta dose rate.

are likely to be less elongated. With these two known limitations, the model is most robust for the bottom right of the contour plots (Fig. 2), and least robust for the top left. In a further limitation, it is assumed all shells within a simulation run are the same size. While this is obviously a simplification, sorting does occur in fluvial and aeolian sedimentation, as it does in shell midden formation, and it is the order-of-magnitude differences in shell size that are of concern here.

In designing a decision strategy for samples with shell material, it should be noted that the external beta dose to quartz grains contributes $\sim 60\%$ of the annual dose. For feldspar, the relative contribution of external beta dose will be lower ($< \sim 50\%$) due to an additional component of internal beta radiation. An error of 5% in the external beta dose rate therefore equates to $\sim 3\%$ error in the total dose rate and age estimate for quartz, and $< 2.5\%$ for feldspar. Given the other sources of uncertainty in OSL dating, a 3% error in the age can usually be tolerated. A decision strategy can then ascertain whether this tolerance is exceeded. The strategy can be demonstrated by considering shell material of three different sizes, each indicated on Fig. 2:

1. *Medium to large shells (volume per shell $> \sim 1 \text{ cm}^3$).* If the pieces of shell material are relatively large, then the beta dose to the sand is similar to the sand-IM dose. With reference to Fig. 2b, a mass fraction of medium to large shells of up to 30% will result in a tolerable error in the beta dose of under 5%, provided that the beta dose measurements are performed on the sand fraction.
2. *Fine shell fragments (volume per fragment $< \sim 0.001 \text{ cm}^3$).* Fine shell fragments have little effect on the bulk-IM dose rate. The error on the bulk-IM dose rate is tolerable for a mass fraction up to $\sim 25\%$. In most cases therefore, fine shell fragments can be included in beta dose measurements.

3. *Shell hash.* Shell material with the size range of shell hash presents a problem. If the total shell mass is $> 10\%$, both the bulk-IM dose rate and the sand-only IM dose rate result in a significant error. For example, a shell-hash mass fraction of 30% will create $\sim 20\%$ error in the beta dose rate, whether or not the shells are included in the beta-dose measurements. A correction will then be required.

Figure 3 shows a graphical visualisation of this decision strategy. Required beforehand are the mass fraction of the shell material (i.e. mass of the $> 1 \text{ mm}$ fraction, divided by the total sediment mass), and the approximate volume of the individual shell fragments (e.g. $A \times B \times C$ axes of a fragment, or its mass in grams divided by 2.71). If the shell material is large or very fine, then the resulting strategy is straightforward. Shell fragments of the size found in shell hash will demand a correction be applied to the dose rate. A rough correction could be made using Fig. 2a or Fig. 2b; a more precise correction would require a sample-specific Monte Carlo model.

6. Conclusion

Discrete shells or shell fragments in sediment create an error in the beta dose rate estimate to quartz or feldspar grains used as dosimeters. This error occurs whether or not the shells are included in the homogenised measurements for beta dose-rate assessment. If shells are medium-sized or larger ($> \sim 1 \text{ cm}^3$), the error is probably tolerable if they are removed from the sample before homogenisation. Fine shell fragments (passing 2 mm sieve) can usually be homogenised with the bulk sample. If small shells or shell-hash sized fragments are present at a mass fraction of $> 10\%$, the beta dose rate will need to be corrected.

If shell material is present, it is straightforward to record its total mass and the approximate size of the shells. With this information, the decision strategy in this paper can be used. In most cases a tolerable error can be achieved without need for correction, but in some cases the correction to the beta dose rate will be required. However, even a small correction may be beneficial; for example, variability in the shell content within a set of samples, if uncorrected for, would create additional sample-to-sample scatter in the age.

Acknowledgments

My thanks to Didier Miallier for reviewing the manuscript, and to Jakob Wallinga for commenting on the draft.

References

- Aitken, M. J. *Aitken Thermoluminescence Dating*. Academic Press Inc, London ; Orlando, October 1985. ISBN 978-0-12-046381-7.
- Ballarini, M., Wallinga, J., Murray, A. S., Van Heteren, S., Oost, A. P., Bos, A. J. J., and Van Eijk, C. W. E. *Optical dating of young coastal dunes on a decadal time scale*. *Quaternary Science Reviews*, 22(10): 1011–1017, 2003.
- Bateman, M. D., Carr, A. S., Murray-Wallace, C. V., Roberts, D. L., and Holmes, P. J. *A dating intercomparison study on Late Stone Age coastal midden deposits, South Africa*. *Geoarchaeology*, 23(6): 715–741, November 2008. doi: 10.1002/gea.20243.
- Briesmeister, J. F. *MCNP-A General Monte Carlo Code N-Particle Transport Code Version 4C*. LA-13709-M, Los Alamos National Laboratory, 2000.
- Cunningham, A. C., Bakker, M. A., van Heteren, S., van der Valk, B., van der Spek, A. J., Schaart, D. R., and Wallinga, J. *Extracting storm-surge data from coastal dunes for improved assessment of flood risk*. *Geology*, 39(11): 1063–1066, 2011.
- Guérin, G., Mercier, N., Nathan, R., Adamiec, G., and Lefrais, Y. *On the use of the infinite matrix assumption and associated concepts: A critical review*. *Radiation Measurements*, 47(9): 778–785, September 2012. doi: 10.1016/j.radmeas.2012.04.004.
- Nathan, R. P. and Mauz, B. *On the dose-rate estimate of carbonate-rich sediments for trapped charge dating*. *Radiation Measurements*, 43(1): 14–25, January 2008. doi: 10.1016/j.radmeas.2007.12.012.
- Nathan, R. P., Thomas, P. J., Jain, M., Murray, A. S., and Rhodes, E. J. *Environmental dose rate heterogeneity of beta radiation and its implications for luminescence dating: Monte Carlo modelling and experimental validation*. *Radiation Measurements*, 37(4): 305–313, 2003.
- Oliver, T. S., Dougherty, A. J., Gliganic, L. A., and Woodroffe, C. D. *Towards more robust chronologies of coastal progradation: Optically stimulated luminescence ages for the coastal plain at Moruya, south-eastern Australia*. *The Holocene*, 25(3): 536–546, March 2015. doi: 10.1177/0959683614561886.
- Pluckhahn, T. J., Hodson, A. D., Rink, W. J., Thompson, V. D., Hendricks, R. R., Doran, G., Farr, G., Cherkinsky, A., and Norman, S. P. *Radiocarbon and luminescence age determinations on Mounds at Crystal River and Roberts Island, Florida, USA*. *Geoarchaeology*, 30(3): 238–260, 2015.
- van Heteren, S., Huntley, D. J., van de Plassche, O., and Lubberts, R. K. *Optical dating of dune sand for the study of sea-level change*. *Geology*, 28(5): 411–414, 2000.
- Zander, A., Degering, D., Preusser, F., Kasper, H. U., and Brckner, H. *Optically stimulated luminescence dating of sublittoral and intertidal sediments from Dubai, UAE: Radioactive disequilibria in the uranium decay series*. *Quaternary Geochronology*, 2(14): 123–128, 2007. doi: 10.1016/j.quageo.2006.04.003.

Reviewer

Didier Miallier